Transient transport properties induced by laser pulses in organic molecular junctions*

HUO Jingyi, LU Qiuxia, ZHANG Maomao, LIU Xiaojing*, AN Zhong*

Hebei Advanced Thin Film Laboratory, Department of Physics, Hebei Normal University, Shijiazhuang 050024, China

Abstract

The time-dependent response of transient current to incident laser pulses in molecular junctions is an important method to obtain the information about molecular structures and excited-state dynamics. In this work, the transient charge transport is studied theoretically through a model polyacetylene molecular junction driven by Gaussian-type femtosecond laser pulses. The molecule is described by the extended Su-Schrieffer-Heeger model, which explicitly includes electron-phonon interactions and involves both electronic and lattice degrees of freedom. The transient transport dynamics are calculated by combining the non-equilibrium Green's function formalism with the hierarchical equations of motion, enabling a fully non-adiabatic description of the coupled electron-lattice evolution.

The results show that the central frequency of the incident laser pulse is one of the key factors affecting the transient current response. When electrons resonate with the optical field, the current amplitude is significantly enhanced, and the temporal profile becomes asynchronous with the laser field, indicating strong non-linear response. The corresponding current spectra exhibit broadened main peaks accompanied by multiple sidebands, suggesting the coexistence of various frequency components due to dynamic coupling between electrons and lattice vibrations.

Further analysis of the evolution of instantaneous energy levels demonstrates that, under resonant excitation, electrons are efficiently excited from the highest occupied molecular orbital (HOMO) to the lowest unoccupied molecular orbital (LUMO). The excited electrons induce lattice relaxation through electron–phonon coupling, resulting in local structural distortion and the formation of self-trapped excitonic

* The paper is an English translated version of the original Chinese paper published in Acta Physica Sinica. Please cite the paper as: HUO Jingyi, LU Qiuxia, ZHANG Maomao, LIU Xiaojing*, AN Zhong*, Transient transport properties induced by laser pulses in organic molecular junctions. *Acta Phys. Sin.*, 2026, 75(2):020703. doi: 10.7498/aps.75.20251125

states. These excitonic effects lead to additional energy transfer channels, thus amplifying the current response and broadening the frequency spectrum.

In contrast, when the lattice motion is artificially frozen, both the current amplitude and frequency broadening are greatly suppressed, and only a single sharp spectral peak corresponding to the laser frequency is observed. This comparison clearly demonstrates that electron-phonon coupling is a key factor governing the transient transport behavior in molecular junctions under optical excitation.

This study reveals the microscopic mechanism of light-induced transient transport in organic molecular junctions and highlights the essential role of lattice dynamics in modulating non-equilibrium charge transfer. These findings provide theoretical guidance for designing novel optoelectronic molecular devices and contribute to the fundamental understanding of non-adiabatic transport processes in low-dimensional quantum systems.

Keywords: molecular junction; electron-phonon coupling; transient transport; photoinduced current;

PACS: 71.38.-k; 72.40.+w; 72.80.Le; 73.63.-b

DOI:10.7498/aps.75.20251125

CSTR: 32037.14.aps.75.20251125

1 Introduction

Molecular junctions[1-4], formed by connecting individual molecules to electrodes, serve as fundamental building blocks for molecular optoelectronic devices. Typically, molecular junctions exhibit high sensitivity to changes in their external environment. Studies demonstrate that photoexcitation can significantly modulate the electronic structure of molecular junctions, thereby influencing their conductance properties while simultaneously offering the distinct advantages of rapid response and high selectivity. These characteristics endow molecular junctions with the potential to function as highly controllable, switchable nanodevices under optical modulation [5,6].

In recent years, numerous experimental studies have uncovered rich physical phenomena in molecular junctions under light irradiation. For instance, light can drive isomerization reactions in molecular structures[7-12]. Several research groups have found that when diarylethene molecules are connected between electrodes to form molecular junctions, reversible switching between open-ring and closed-ring isomers can be achieved under illumination[7-10]. This structural transformation induces conductance changes across the molecule and electrodes, thereby realizing

single-molecule switching functionality. Similarly, the conductance difference between trans and cis isomers constitutes a core mechanism for light-driven molecular switches. Cao et al.[11] first demonstrated reversible conductance switching of a single azobenzene molecule between cis and trans conducting states under alternating ultraviolet and visible light irradiation. By optimizing electrode geometry and selecting appropriate anchoring groups, the stability and reversibility of molecular switches can be effectively enhanced, enabling efficient optically controlled switching[12].

Another class of experiments reveals that light-molecule coupling can also significantly alter the conductance of molecular junctions through photoconductive mechanisms[13-17]. Battacharyya et al.[13] observed that under visible light irradiation, the conductance of porphyrin-fullerene molecules increases due to photoinduced electron transfer, reverting to its initial state in the dark. In structurally symmetric molecular junctions, Zhou et al.[14] measured conductance under both dark and illuminated conditions, confirming that photoexcitation enhances conductance by approximately 40% via exciton state formation. Furthermore, light fields can induce photon-assisted tunneling effects[15,16], exhibiting high sensitivity to the wavelength of incident light[17]. Recently, Lee et al.[18,19] introduced monochromatic light illumination from the glass side of organic field-effect transistors and found that the drain current increases with light intensity. This indicates that photogenerated charges facilitate electron transport between source and drain, enabling the device to exhibit favorable output characteristics even at low gate voltages. Further investigations show that increasing light intensity enhances conductance and reduces the threshold voltage, thereby achieving effective modulation of photocurrent relative to dark current. These experimental results confirm that molecular junctions driven by light fields possess excellent rapid responsiveness and high selectivity, establishing them as a crucial platform for exploring single-molecule optoelectronic functionalities.

On the theoretical side, researchers have conducted extensive work within a quantum mechanical framework to elucidate the microscopic mechanisms underlying light-molecular junction interactions. Galperin et al.[20-23] employed a molecular HOMO (the highest occupied molecular orbital)/LUMO (the lowest unoccupied molecular orbital) model to describe molecules exhibiting significant dipole moment changes during excitation, demonstrating that photoexcitation can induce photocurrent even without an external bias. Cao et al.[24] combined first-principles calculations with the non-equilibrium Green's function (NEGF) method to simulate transient currents in Au-benzene-Au molecular junctions under Gaussian laser pulses, finding that current amplitude reaches a maximum and decays most slowly in the resonance region. Zhou et al.[14] constructed a simple molecular junction transport model and showed that when the light frequency approaches the HOMO-LUMO gap of the molecule, exciton state

formation shifts energy levels and enhances electrical response. Beltako et al.[25] investigated donor-acceptor interfacial systems and revealed that both exciton states and charge-transfer states can significantly influence photoinduced currents. Additionally, Selzer and Peskin[26] achieved transient current multiplication through multipulse excitation. These studies collectively uncover diverse mechanisms of electronic excitation and charge transport in molecular junctions under light fields. However, several knowledge gaps remain regarding quantum transport processes driven by light fields. Most studies focus on quantum transport under steady-state conditions[14,20-22], whereas molecular junctions under rapidly varying light fields often reside in a non-equilibrium transient regime, where current exhibits strong fluctuations that steady-state analyses cannot fully capture. Moreover, most organic molecules possess quasi-one-dimensional structures, and strong electron-phonon coupling significantly affects transport dynamics. Existing studies indicate that electron-phonon interactions not only determine steady-state current characteristics but may also induce current oscillations and localized state formation in transient dynamics[27]. Although methods combining NEGF with molecular dynamics can partially address molecule-electrode coupling and dissipative effects[24-26], describing non-equilibrium charge transport under strong electron-phonon coupling remains challenging. Therefore, constructing a theoretical framework that simultaneously accounts for non-equilibrium dynamics, electron-phonon interactions, and strong-field excitation effects is essential for revealing the quantum transport mechanisms of molecular junctions under light-field driving.

Building upon this background, this study constructs an organic molecular junction system composed of metal-polyacetylene-metal. We employ the Su-Schrieffer-Heeger (SSH) model to characterize electron-phonon coupling within the organic molecule. By combining NEGF with hierarchical equations of motion (HEOM) to solve the evolution of electronic states and lattice degrees of freedom, and incorporating non-adiabatic molecular dynamics, we simulate and analyze the transient response characteristics of the system under Gaussian laser pulse excitation, thereby elucidating the cooperative mechanism between photoexcitation and electron-phonon coupling.

2 Hamiltonian and Computational Methods for Transient Quantum Transport in Open Systems

2.1 Hamiltonian of the Quantum Transport System

Under laser pulse irradiation, the Hamiltonian of the molecular junction comprises the following four components:

$$H = H_S + H_B + H_{SB} + H_{ext}, \quad (1)$$

Among these, the Hamiltonian H_S describes the electronic structure of the polyacetylene molecular chain. To elucidate the conduction mechanism of trans-polyacetylene, Su et al.[28] proposed the Su-Schrieffer-Heeger (SSH) model in 1979. This model fully accounts for electron-phonon coupling effects and has achieved widespread success in theoretical studies of the electrical properties of organic polymers. To further characterize organic molecular systems with non-degenerate ground states, this study incorporates a degeneracy-breaking term[29] and employs an extended SSH model to describe the organic molecule, expressed as

$$\begin{aligned} H_S = & -\sum_n [t_0 - \beta(u_{n+1} - u_n) - (-1)^n t_e](a_{n+1}^\dagger a_n \\ & + \text{h.c.}) + \frac{K}{2}\sum_n (u_{n+1} - u_n)^2 + \frac{M}{2}\sum_n \dot{u}_n^2, \end{aligned} \quad (2)$$

Here, t_0 denotes the hopping integral between nearest-neighbor atoms in the equilibrium atomic lattice, u_{n+1} and u_n represent the displacements of the $n+1$th and n th lattice atoms from their equilibrium positions, respectively, β is the electron-phonon coupling strength, t_e is the degeneracy-breaking parameter, $a_{n+1}^\dagger (a_n)$ ($\dot{u}_n$) is the electron creation (annihilation) operator, K is the elastic constant, M is the mass of the lattice atom, and $\dot{n}$ is the velocity of the n th lattice atom.

The second term in Eq. (1), H_B, represents the Hamiltonian of the electrodes, which we describe using a non-interacting fermion model. Its explicit form is

$$H_B = \sum_{\alpha=L,R} \sum_k [\varepsilon_{\alpha k} + \Delta_\alpha(t)]\, d_{\alpha k}^\dagger d_{\alpha k}, \quad (3)$$

Here, α denotes the left or right electrode, $\varepsilon_{\alpha k}$ represents the single particle of electrons with momentum k in electrode α at equilibrium, $\Delta_\alpha(t)$ denotes the time-dependent component of the single-electron energy in the electrode, and $d_{\alpha k}^\dagger$ and $d_{\alpha k}$ are the creation and annihilation operators, respectively, for electrons in electrode α.

The third term in Equation (1), H_{SB}, represents the molecule-electrode coupling Hamiltonian, which takes the following explicit form:

$$H_{SB} = \sum_\alpha \sum_{k,n} (V_{\alpha k,n} d_{\alpha k}^\dagger a_n + \text{h.c.}), \quad (4)$$

Here, $V_{\alpha k,n}$ denotes the coupling coefficient between the molecule and the electrode. In numerical simulations, the left electrode couples exclusively to the first atomic site of the molecule ($n = 1$), while the right electrode couples solely to the last atomic site ($n = N$), i.e., $V_{Lk,1} = V_{Rk,N} \neq 0$.

We employ a Gaussian envelope approximation to model the electric field generated by the laser pulse within the molecule[30], which takes the following form:

$$E(t) = E_0 \mathrm{e}^{-[(t-\tau_0)/\tau]^2} \sin(\omega t), \tag{5}$$

Here, τ_0 denotes the center of the applied laser pulse, τ represents its duration-specifically, i.e., the half-width of the Gaussian function, the central frequency of the optical pulse is ω, and its intensity is E_0.

The direction of the optical field is aligned parallel to the molecular junction. Following the application of the optical field, the Hamiltonian describing the interaction among light, electrons, and the lattice within the molecule can be expressed as

$$H_{\mathrm{ext}} = eE(t) \sum_n (na + u_n)(a_n^{\dagger} a_n - 1), \tag{6}$$

Here, a denotes the lattice constant, i.e., the interatomic distance when atoms are arranged with uniform spacing.

2.2 Cascaded Equations of Motion

When investigating the dynamical evolution of electrons in open quantum systems, the most critical component is the system's reduced density matrix. By employing the nonequilibrium Green's function (NEGF) method in conjunction with the hierarchical equations of motion (HEOM)[31-33], one can derive the equation of motion for the reduced density matrix of a molecular junction, thereby effectively describing the system's dynamical behavior.

The reduced density matrix of the system, $\boldsymbol{\rho}(t)$, is related to the Green's function $\boldsymbol{G}^{<}(t,t')$ as follows:

$$\dot{\boldsymbol{\rho}}(t) = -\mathrm{i}\hbar \dot{\boldsymbol{G}}^{<}(t;t). \tag{7}$$

According to the Dyson equation and the Keldysh equation[34], the time derivative of the Green's function $\boldsymbol{G}^{<}(t,t')$ can be obtained:

$$\begin{aligned} \mathrm{i}\hbar \frac{\partial \boldsymbol{G}^{<}(t,t')}{\partial t} = \boldsymbol{h}(t)\boldsymbol{G}^{<}(t,t') + \int_{-\infty}^{\infty} [\boldsymbol{\Sigma}^{<}(t,t_1) \\ \times \boldsymbol{G}^{\mathrm{a}}(t_1,t') + \boldsymbol{\Sigma}^{\mathrm{r}}(t,t_1)\boldsymbol{G}^{<}(t_1,t')]\mathrm{d}t_1, \end{aligned} \tag{8}$$

$$\begin{aligned} \mathrm{i}\hbar \frac{\partial \boldsymbol{G}^{<}(t,t')}{\partial t'} = -\boldsymbol{G}^{<}(t,t')\boldsymbol{h}(t') - \int_{-\infty}^{\infty} [\boldsymbol{G}^{\mathrm{r}}(t,t_1) \\ \times \boldsymbol{\Sigma}^{<}(t_1,t') + \boldsymbol{G}^{<}(t,t_1)\boldsymbol{\Sigma}^{\mathrm{a}}(t_1,t')]\mathrm{d}t_1, \end{aligned} \tag{9}$$

Here, $\boldsymbol{\Sigma}^{\mathrm{a}/<}(t,t_1)$ denotes the self-energy of the electrode, and $\boldsymbol{h}(t)$ represents the

matrix of the electronic part of the Hamiltonian for the molecule, encompassing both the electronic component of the organic molecule and the optical field component. Substituting Equations (8) and (9) into Equation (7) yields the evolution equation for the reduced density matrix:

$$\mathrm{i}\hbar\dot{\boldsymbol{\rho}}(t) = [\boldsymbol{h}(t), \boldsymbol{\rho}(t)] - \sum_{\boldsymbol{\alpha}} [\boldsymbol{\varphi}_{\boldsymbol{\alpha}}(t) - \boldsymbol{\varphi}_{\boldsymbol{\alpha}}^{\dagger}(t)], \tag{10}$$

where $\boldsymbol{\varphi}_{\boldsymbol{\alpha}}(t)$ denotes the first-order adjoint density matrix, whose explicit form is

$$\begin{aligned} \boldsymbol{\varphi}_{\boldsymbol{\alpha}}(t) = & -\mathrm{i}\hbar \int_{-\infty}^{\infty} [\boldsymbol{G}^{\mathrm{r}}(t,t_1)\boldsymbol{\Sigma}_{\boldsymbol{\alpha}}^{<}(t_1,t) \\ & + \boldsymbol{G}^{<}(t,t_1)\boldsymbol{\Sigma}_{\boldsymbol{\alpha}}^{\mathrm{a}}(t_1,t)]\mathrm{d}t_1, \\ \boldsymbol{\varphi}_{\boldsymbol{\alpha}}^{\dagger}(t) = - & \mathrm{i}\hbar \int_{-\infty}^{\infty} [\boldsymbol{\Sigma}_{\boldsymbol{\alpha}}^{<}(t,t_1)\boldsymbol{G}^{\mathrm{a}}(t_1,t) \\ & + \boldsymbol{\Sigma}_{\boldsymbol{\alpha}}^{\mathrm{r}}(t,t_1)\boldsymbol{G}^{<}(t_1,t)]\mathrm{d}t_1. \end{aligned} \tag{11}$$

Using the relation

$X^{r/a}(t,\tau) = \pm\theta[\pm(t-\tau)][X^{>}(t,\tau) - X^{<}(t,\tau)]$, where X stands for $\boldsymbol{G}$ or $\boldsymbol{\Sigma}_{\alpha}$, substituting into equation (11) yields the specific forms of $\boldsymbol{\varphi}_{\boldsymbol{\alpha}}(t)$ and $\boldsymbol{\varphi}_{\boldsymbol{\alpha}}^{\dagger}(t)$:

$$\begin{aligned} \boldsymbol{\varphi}_{\boldsymbol{\alpha}}(t) = & \mathrm{i}\hbar \int_{-\infty}^{\infty} \theta(t-t_1)[\boldsymbol{G}^{<}(t,t_1)\boldsymbol{\Sigma}_{\boldsymbol{\alpha}}^{>}(t_1,t) \\ & - \boldsymbol{G}^{>}(t,t_1)\boldsymbol{\Sigma}_{\boldsymbol{\alpha}}^{<}(t_1,t)]\mathrm{d}t_1, \\ \boldsymbol{\varphi}_{\boldsymbol{\alpha}}^{\dagger}(t) = & -\mathrm{i}\hbar \int_{-\infty}^{\infty} \theta(t-t_1)[\boldsymbol{\Sigma}_{\boldsymbol{\alpha}}^{>}(t,t_1)\boldsymbol{G}^{<}(t_1,t) \\ & - \boldsymbol{\Sigma}_{\boldsymbol{\alpha}}^{<}(t,t_1)\boldsymbol{G}^{>}(t_1,t)]\mathrm{d}t_1, \end{aligned} \tag{12}$$

Here, $\theta(t-t_1)$ denotes the Heaviside step function.

Under the wide-band approximation, the broadening function is assumed to be independent of the energy of electrons in the electrode, and the self-energy can be expressed as

$$\begin{aligned} \boldsymbol{\Sigma}_{\alpha}^{<}(t_1,t) = & \boldsymbol{J}^{\alpha}\exp[\tfrac{\mathrm{i}}{\hbar}\int_{t_1}^{t} \Delta_{\alpha}(\tau)\mathrm{d}\tau] \\ & \times \tfrac{\mathrm{i}}{\hbar}\int_{0}^{\infty} f_{\alpha}(\varepsilon)\mathrm{e}^{\frac{\mathrm{i}}{\hbar}\varepsilon(t-t_1)}\mathrm{d}\varepsilon, \\ \boldsymbol{\Sigma}_{\alpha}^{>}(t_1,t) = & -2\pi\mathrm{i}\exp(\tfrac{\mathrm{i}}{\hbar}\int_{t_1}^{t} \Delta_{\alpha}(\tau)\mathrm{d}\tau) \\ & \times \delta(t-t_1) + \boldsymbol{\Sigma}_{\alpha}^{<}(t_1,t), \end{aligned} \tag{13}$$

Here, $f_{\alpha}(\varepsilon)$ denotes the Fermi distribution function, and $\boldsymbol{J}^{\alpha}$ represents the matrix of the broadening function, whose matrix elements are given by $J_{nm}^{\alpha}(\varepsilon_{\alpha k}) = \rho(\varepsilon_{\alpha k})V_{\alpha k,n}^{*}V_{\alpha k,m}$, where $\rho(\varepsilon_{\alpha k})$ is the electronic density of states in the one-dimensional electrode. Substituting Equation (13) into Equation (12) yields the following expression for the first-tier auxiliary density matrix:

$$\boldsymbol{\varphi}_{\alpha}(t) = \mathrm{i}\pi\boldsymbol{\rho}(t)\boldsymbol{J}^{\alpha} + \int_{0}^{\infty} \boldsymbol{\varphi}_{\alpha}(\varepsilon,t)\mathrm{d}\varepsilon, \tag{14}$$

Among these

$$\boldsymbol{\varphi}_{\alpha}(\varepsilon,t) = -\mathrm{i}\hbar\int_{-\infty}^{\infty} \boldsymbol{G}^{\mathrm{r}}(t,t_1)\boldsymbol{\Sigma}_{\alpha}^{<}(t_1,t,\varepsilon)\mathrm{d}t_1. \tag{15}$$

By leveraging the time evolution of $\boldsymbol{G}^{\mathrm{r}}$ and $\boldsymbol{\Sigma}_{\alpha}^{<}$, we obtain the evolution equations for $\boldsymbol{\varphi}_{\alpha}(\varepsilon,t)$ and $\boldsymbol{\varphi}_{\alpha}^{\dagger}(\varepsilon,t)$ as follows:

$$\begin{aligned}
\mathrm{i}\hbar\dot{\boldsymbol{\varphi}}_{\alpha}(\varepsilon,t) = \quad & \boldsymbol{J}^{\alpha} f_{\alpha}(\varepsilon) + [\boldsymbol{h}(t) - \varepsilon - \Delta_{\alpha}(t) \\
& -\mathrm{i}\pi(\boldsymbol{J}^{\mathrm{L}} + \boldsymbol{J}^{\mathrm{R}})]\boldsymbol{\varphi}_{\alpha}(\varepsilon,t), \\
\mathrm{i}\hbar\dot{\boldsymbol{\varphi}}_{\alpha}^{\dagger}(\varepsilon,t) = \quad & -f_{\alpha}(\varepsilon)\boldsymbol{J}^{\alpha} - \boldsymbol{\varphi}_{\alpha}^{\dagger}(\varepsilon,t)[\boldsymbol{h}(t) - \varepsilon \\
& -\Delta_{\alpha}(t) + \mathrm{i}\pi(\boldsymbol{J}^{\mathrm{L}} + \boldsymbol{J}^{\mathrm{R}})].
\end{aligned} \tag{16}$$

At this point, the set of evolution equations for the electronic states-comprising Equations (10), (14), and (16) form a closet set of equations. Solving these equations simultaneously yields the time evolution of the electron density.

From this result, one can further compute the transient current flowing from electrode α into the polyacetylene molecule, which is expressed as

$$I_{\alpha}(t) = \frac{\mathrm{d}\langle N_{\alpha}\rangle}{\mathrm{d}t} = \frac{\mathrm{i}e}{\hbar}\sum_{n,\varepsilon}[\varphi_{n,\alpha n}(\varepsilon,t) - \varphi_{n,\alpha n}^{\dagger}(\varepsilon,t)], \tag{17}$$

Here, $\langle N_{\alpha}\rangle$ denotes the number of electrons in electrode α, and $\varphi_{n,\alpha n}(\varepsilon,t)$ represents the matrix element of $\boldsymbol{\varphi}_{\alpha}(\varepsilon,t)$ in Equation (15).

The evolution of lattice atoms is treated using classical mechanics, and their equations of motion are derived from Newton's second law:

$$\begin{aligned}
M\ddot{u}_n(t) = \quad & -K[2u_n - u_{n+1} - u_{n-1}] \\
& +\beta[\rho_{n,n+1} + \rho_{n+1,n} - \rho_{n-1,n} - \rho_{n,n-1}] \\
& -eE(t)(\rho_{n,n} - 1),
\end{aligned} \tag{18}$$

Here, $\rho_{n,n+1}$, $\rho_{n,n-1}$, and $\rho_{n,n}$ denote the elements of the reduced density matrix.

Owing to the coupling between electronic and lattice states during system evolution, we solve the coupled equations of motion-specifically, the electronic equations (10), (14), and (16), together with the lattice evolution equation (18)-to determine the dynamical states of both electrons and the lattice at any given time. This approach enables us to obtain the transient response characteristics of polyacetylene molecules under laser pulse excitation. All numerical simulations in this study were performed using the MATLAB platform. We employed the ode45 algorithm to integrate the coupled differential equations governing the dynamical evolution, thereby capturing the time-dependent behavior of both electronic and lattice states.

3 Results and Discussion

To align the band structure of the polyacetylene molecular chain with experimental data and first-principles calculations, we adopt the following parameter values in the Hamiltonian: $t_0 = 2.5\text{eV}$, $\beta = 4.1\text{eV/Å}$, $K = 21.0\text{eV/Å}^2$, $M = 1349.14\text{eV}\cdot\text{fs}^2/\text{Å}^2$, $t_e = 0.01\text{eV}$, and $a = 1.22\text{Å}$. We consider a polyacetylene chain comprising 24 (CH) units as our model system, bridged between two semi-infinite metallic electrodes. These electrodes act as fermionic reservoirs, and the system temperature is set to room temperature ($T = 300\text{K}$). Since the electrodes couple only to the first and last atoms of the molecular chain, the non-zero matrix elements in the broadening function $\boldsymbol{J}^{\alpha}$ are set to $J_{11} = J_{NN} = 0.05\text{eV}$. As shown in Fig. 1(a), the bridged molecule exhibits a characteristic alternating short-long bond structure-a consequence of electron-phonon coupling inducing dimerization in the one-dimensional chain, which opens an energy gap. Figure 1(b) displays the molecular eigenenergy spectrum, where the HOMO (highest occupied molecular orbital) is indicated by a solid blue line and the LUMO (lowest unoccupied molecular orbital) by a solid red line. The energy difference between them is 1.76eV, defining the bandgap width. Due to the particle-hole conjugation symmetry inherent in the Su-Schrieffer-Heeger (SSH) model Hamiltonian, the energy bands are symmetric about $E = 0\text{eV}$.

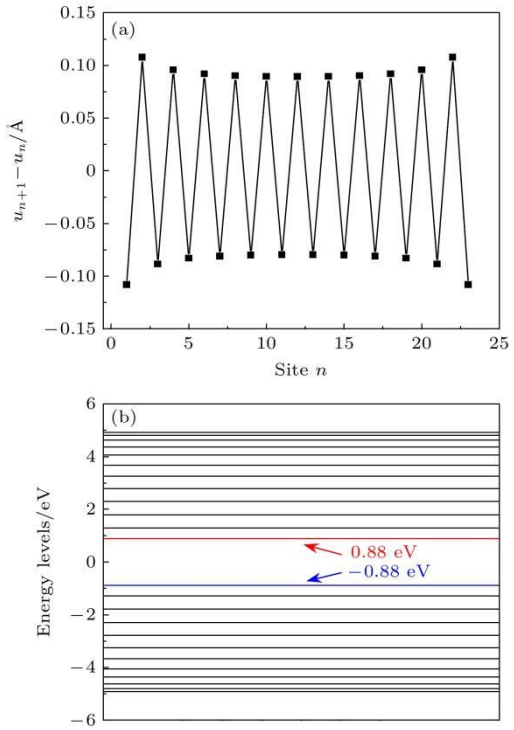

Fig. 1 (a) The lattice configuration and (b) energy levels of the bridged molecule.

When the energy of the incident light field exactly equals the material bandgap E_g, the central frequency ω of the optical pulse under this condition is defined as the critical

frequency ω_C. Based on the parameters established earlier, the bandgap of polyacetylene and its corresponding critical frequency are $\hbar\omega_C = E_g = 1.76\text{eV} \rightarrow \omega_C = 2.67\text{rad/fs}$. The optical pulse is set with a central time $\tau_0 = 150\text{fs}$, duration $\tau = 50\text{fs}$, and peak amplitude $E_0 = 0.05\text{V/Å}$. We next simulate the transient response of the molecular junction under laser pulses with different central frequencies.

Figure 2 presents the time evolution of the molecular junction current (Fig. 2(a1)-(d1)) and the corresponding spectral distributions (Fig. 2(a2)-(d2)) under optical pulses with varying central frequencies. When the central frequency of the incident light is low, $\omega = 0.7\omega_C$ (Fig. 2(a1)), the corresponding photon energy ($0.7E_g$) is below the material bandgap. The current remains nearly synchronized with the optical field, exhibits a small amplitude, and decays rapidly after the pulse ends. The corresponding spectrum in Fig. 2(a2) shows only a single weak peak at the incident light frequency, indicating a weak system response and confirming that the system operates in the linear response regime. When the excitation frequency increases to $\omega = 0.8\omega_C$ (Fig. 2(b1)), the photon energy reaches $0.8E_g$, and the current amplitude increases significantly. Notably, after approximately 130 fs, the temporal evolution of the current deviates from the Gaussian pulse envelope, exhibiting a phase lag and complex oscillations, indicating loss of strict synchronization with the optical field. Oscillations persist even after the optical pulse has decayed to zero. The corresponding spectrum (Fig. 2(b2)) displays a broadened main peak accompanied by secondary peaks, with substantially enhanced intensity, revealing richer frequency components in the current signal and reflecting strong resonant responses across a broader frequency range. Further increasing the central frequency to $1.0\omega_C$ (Fig. 2(c1)) results in a current waveform that diverges more markedly from the optical field and requires a longer time to decay to zero. Compared with Fig. 2(b1), the maximum current amplitude decreases despite the higher photon energy. The spectral features in Fig. 2(c2) become sharper, and the side peaks weaken significantly relative to Fig. 2(b2), suggesting a more concentrated spectral response. When the excitation frequency corresponds to photon energy above the bandgap (Fig. 2(d1)), the current again synchronizes with the optical field but with reduced amplitude, and the spectrum retains only a single sharp peak (Fig. 2(d2)) with further diminished intensity. In summary, the transient current of the molecular junction exhibits pronounced nonlinear behavior in response to optical frequency: the current response peaks near the bandgap energy, displaying clear resonant characteristics, whereas far from the resonance region, the system primarily demonstrates linear, field-synchronized responses.

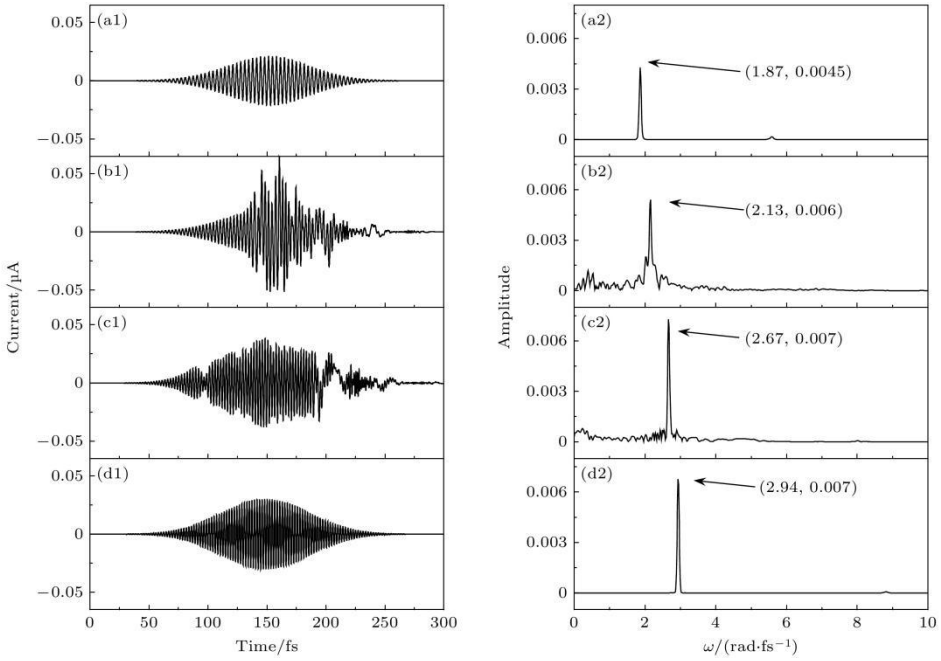

Fig. 2 Response of the transient current in the molecular junction to the laser pulse with various central frequencies: (a) $0.7\omega_C$**; (b)** $0.8\omega_C$**; (c)** $1.0\omega_C$**; (d)** $1.1\omega_C$**.**

To elucidate the physical mechanism underlying the current response differences shown in Figure 2, Figure 3 presents the time evolution of the molecular eigenenergies and their electron occupations under optical pulses with different central frequencies. When the photon energy is either too low or too high (Figures 3(a) and 3(d)), the molecular energy levels exhibit minimal temporal variation, showing only slight convergence near the pulse center, with very few electrons excited, resulting in a weak current response. However, when the central frequency of the optical pulse approaches resonance with the molecular energy gap (Figure 3(b)), the energy-level shift becomes most pronounced. The HOMO and LUMO come closest together at approximately 148 fs, corresponding to the maximum number of excited electrons. The resulting electron-hole pairs induce lattice relaxation through electron-phonon coupling, thereby shifting the HOMO and LUMO positions. Because the optical pulse comprises a broad spectrum of electromagnetic frequencies, this lattice relaxation further modulates the eigenenergy positions, establishing a positive feedback loop that excites additional electrons. Some electrons may even transition to higher-energy orbitals (e.g., HOMO-1 → LUMO+1), leading to sustained energy-level oscillations. Although the optical field decays after 300 fs, these oscillations persist throughout the simulated 1000 fs without damping, reflecting the intrinsic electron-phonon coupling dynamics within the system. After the optical field decays ($t > 150\text{fs}$), some electrons are extracted into the electrodes, causing the electron population on the LUMO to decrease and the current amplitude to gradually diminish. Nevertheless, residual lattice oscillations bring the HOMO and LUMO into proximity again at around 195 fs, triggering a secondary

excitation event and a corresponding minor current rebound. As the optical field continues to decay, no substantial re-excitation of electrons occurs. Following the termination of the optical pulse, the electron occupations on the HOMO and LUMO gradually revert to their pre-excitation distribution, and the system current decays to zero. If the central frequency of the incident light is further increased to $1.0\omega_C$ (Figure 3(c)), the resonance condition is disrupted, electron excitation efficiency declines, and the current response weakens accordingly. Overall, the magnitude of the current response depends critically on the degree of matching between the photon energy and the molecular energy gap. Under resonant conditions, photoexcitation enhances coupling between the HOMO and LUMO, dynamically bringing the energy levels closer together and facilitating electron transitions. Concurrently, electron-phonon interactions further modulate the energy-level positions, generating a synergistic effect that significantly amplifies the current response.

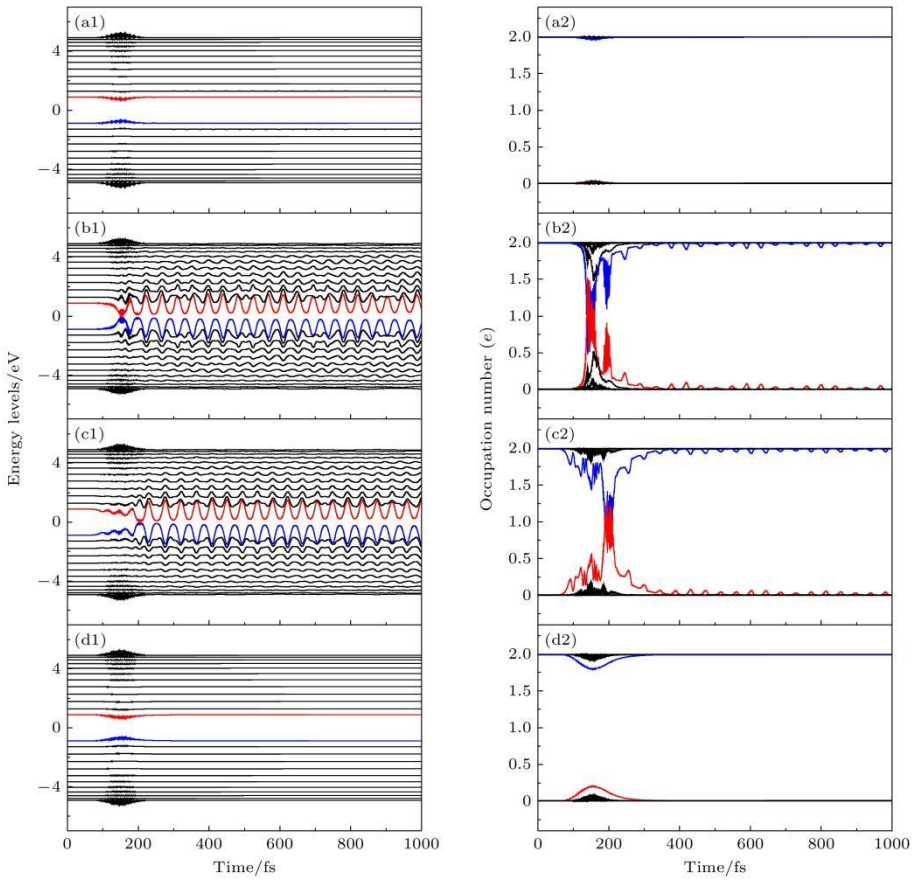

Fig. 3 Time evolution of the molecular energy levels and the corresponding electron occupation number under varying laser pulses: (a) $0.7\omega_C$**; (b)** $0.8\omega_C$**; (c)** $1.0\omega_C$**; (d)** $1.1\omega_C$**.**

Excited electrons undergo relaxation through electron-phonon coupling, thereby inducing changes in the lattice configuration. Figure 4 illustrates the lattice configurations at four specific time points under the influence of a laser pulse with a central frequency of $0.8\omega_C$. The degree of lattice distortion is represented by $y_n =$

$(-1)^n(u_{n+1}-u_n)$ and compared with the initial configuration (black dashed line). As shown in Figure 4(a), near the peak of the optical pulse, significant distortion emerges at the center of the molecular chain, coinciding precisely with the first approach of the HOMO and LUMO and the moment of strongest electronic excitation. At this instant, electron-phonon coupling causes electron localization in the central region of the molecule, resulting in pronounced lattice distortion there. Over time, by t = 180 fs, as depicted in Figure 4(b), electrons and holes flow toward the electrodes, the HOMO and LUMO gradually separate, and the lattice configuration returns to its initial state. When the energy levels approach each other again, as shown in Figure 4(c), partial electrons are re-excited and induce distortion, albeit with markedly reduced amplitude, indicating diminished electronic excitation intensity. Finally, at t = 300 fs, as shown in Figure 4(d), the optical field decays and the HOMO and LUMO separate once more, allowing electron occupation to gradually recover and lattice distortion to correspondingly diminish. It should be noted that at the time corresponding to Figure 4(a), the net charge within the molecule is zero. Combined with Figures 3(b1) and (b2), this indicates a net excitation corresponding to a charge transfer of 1.5e, triggering lattice distortion and forming deep energy levels within the bandgap derived from HOMO and LUMO. The state characterized by localized electron-hole pairs accompanied by lattice distortion demonstrates that the system forms a typical excitonic state at this instant-a direct consequence of the combined effects of photoexcitation and electron-phonon coupling.

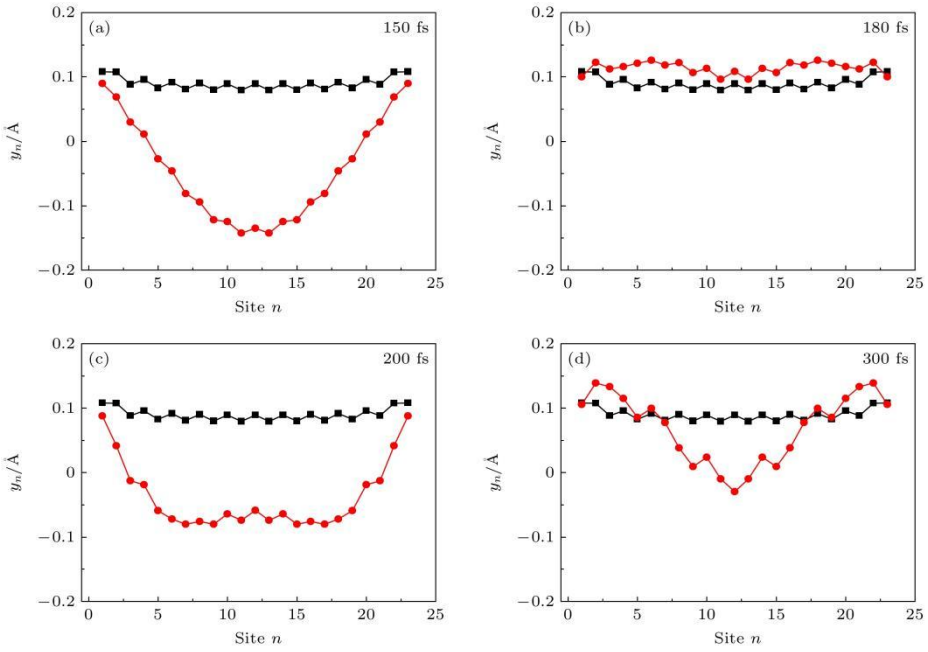

Fig. 4 Transient lattice deformation at specific moments *t* = 150, 180, 200, 300 fs under the action of optical pulses with a central frequency $0.8\omega_C$.

To further investigate the role of electron-phonon coupling in the photoexcited transient response, Figure 5 presents the current and spectral evolution of the molecular junction

under frozen lattice conditions, where atomic motion is suppressed. As shown in Figure 5(a), when lattice vibrations are inhibited, the current response is significantly attenuated and its temporal evolution closely follows the optical field envelope, peaking at approximately 150 fs. The corresponding frequency spectrum, depicted in Figure 5(b), exhibits only a single characteristic peak aligned with the central frequency of the incident light, lacking the multiple frequency components and broadband spectral response observed in Figure 2(b2). This indicates that, with lattice dynamics included, electron-phonon interactions play a pivotal role: lattice distortions dynamically modulate the molecular energy spectrum via feedback, introducing additional frequency components and nonlinear oscillations that subsequently influence electronic excitation and photocurrent generation. Further examination of the energy-level evolution, as shown in Figures 5(c) and (d), reveals that both the intrinsic molecular energy levels and electron occupation numbers exhibit minimal temporal variation when the lattice is frozen. This demonstrates that a rigid lattice cannot respond to energy feedback from photoexcited electrons, resulting in an absence of dynamic spectral modulation. Consequently, self-trapped excitonic states within the bandgap cannot form, leading to a pronounced suppression of further electronic excitation and photocurrent intensity. In summary, electron-phonon coupling enables spectral modulation and nonlinear excitation through dynamic lattice distortions, constituting the primary physical mechanism underlying the strong transient response of molecular junctions to optical fields.

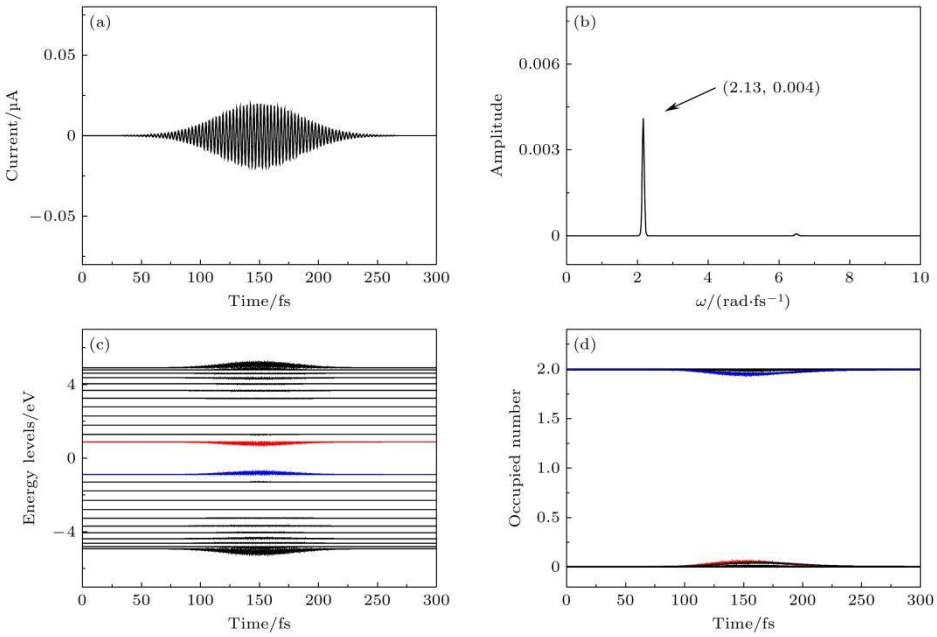

Fig. 5 Time evolution of (a) the current in the molecular junction; (b) frequency spectrum distribution of the time-domain current; (c) the molecular energy levels; (d) the electron occupation number under a laser pulse of $0.8\omega_C$ with the motion of the lattice atoms frozen.

In the aforementioned simulations, the peak amplitude of the optical pulse was set to E_0 = 0.05 V/Å. To further investigate the influence of optical pulse intensity on the transient current response of the molecular junction, we analyzed the variations in response under different amplitudes while keeping the pulse center time and duration constant. Figures 6(a) and (b) display the transient current responses within the molecular junction for peak amplitudes of E_0 = 0.1 V/Å and E_0 = 0.2 V/Å, respectively. Specifically, Figures 6(a1) and (b1) correspond to a central frequency of $0.8\omega_C$, whereas Figures 6(a2) and (b2) correspond to a central frequency of $1.0\omega_C$. The results indicate that as the peak amplitude of the optical pulse field increases, the amplitude of the response current also intensifies. This suggests that during the optical pulse, a higher E_0 increases the effective number of photons available for resonant excitation within the system, thereby exciting more electrons. Under electron-phonon coupling, electron-hole pairs more readily form self-trapped exciton states. This photoinduced excitonic mechanism subsequently contributes to the dynamical evolution of the system and further enhances the current response magnitude.

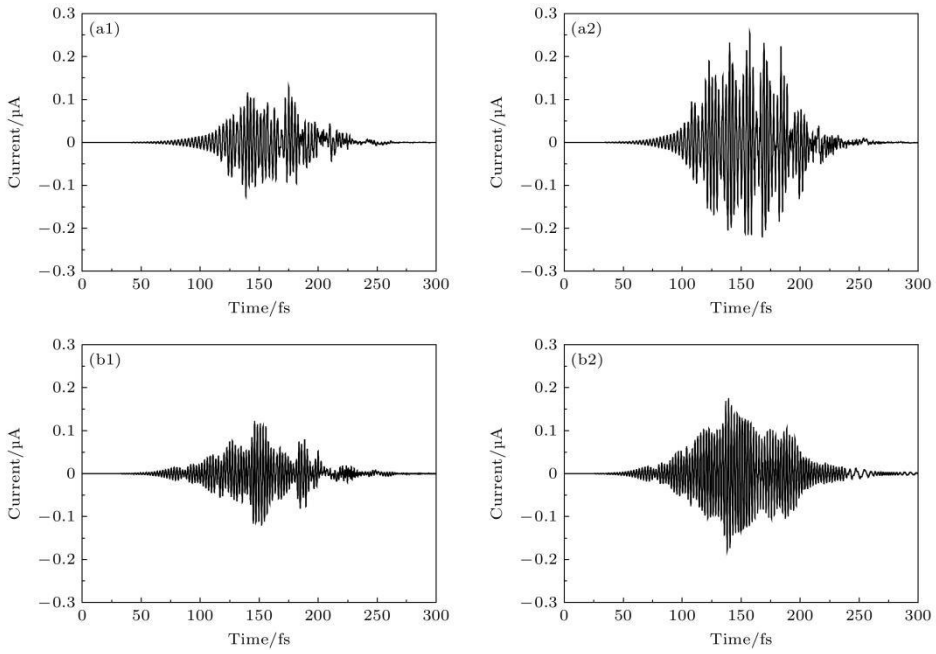

Fig. 6 Response of the transient current in the molecular junction to the laser pulse with various peak amplitudes: (a) E_0 = 0.1 V/Å; (b) E_0 = 0.2 V/Å.

4 Conclusion

This study simulates the transient response characteristics of organic molecular junctions under optical pulse excitation, with a particular focus on the generation mechanism of resonance-induced photocurrent under zero-bias conditions. We primarily investigate the influence of two key factors-the central frequency of the optical pulse and electron-phonon coupling-on the transient current. The results

demonstrate that the optical pulse-induced current exhibits markedly distinct behaviors in off-resonance and resonance regimes. In the off-resonance regime, the number of excited electrons remains limited, and the current response remains synchronized with the optical field variation. In contrast, within the resonance regime, a substantially larger population of electrons is excited, leading to a pronounced enhancement in current amplitude, a slower decay process, and a complex temporal evolution that becomes desynchronized from the optical field. Further comparative simulations, in which lattice atomic motion was artificially frozen, reveal that electron-phonon interactions play a pivotal role. Coupling between excited electrons and the lattice triggers lattice dynamical relaxation, which in turn induces periodic oscillations in the intrinsic energy levels over time. This dynamic modulation persists even after the optical pulse ceases, thereby providing a sustained channel for electron excitation. The Gaussian-shaped optical pulse comprises multiple frequency components, which synergistically interact with the intrinsic energy spectrum modified by lattice distortions, thereby enhancing the molecular chain's absorption capability and broadening the frequency range for electron excitation. In the resonance regime, this coupling process leads to the formation of self-trapped excitonic states, causing the current response to lose synchronization with the laser pulse electric field. Moreover, moderately increasing the peak intensity of the optical field significantly boosts the number of excited electrons, thereby enhancing the transient current amplitude. Since the current in molecular junctions constitutes a primary experimentally accessible signal, we anticipate that investigations into the transient current response to incident laser pulses will yield valuable insights into the properties of excited states in molecular junctions and further provide theoretical support for elucidating the fundamental physical mechanisms underlying light-matter interactions.

References

[1] Akkerman H B, Blom P W M, Leeuw D M, Boer B 2006 *Nature* **441** 69

[2] Shekhawat A S, Krishnan N, Diwan A, Murugan D, Chithravel A, Daukiya L, Shrivastav A M, Srivastava T, Saxena S K 2025 *Nanoscale* **17** 8363

[3] Xie Z X, Yu X, Jia P Z, Chen X K, Deng Y X, Zhang Y, Zhou W X 2023 *Acta Phys. Sin.* **72** 124401

[4] Zhang H X, Zhu Y X, Duan P, Shiri M, Yelishala S C, Shen S C, Song Z Q, Jia C C, Guo X F, Cui L J, Wang K 2024 *Appl. Phys. Rev.* **11** 041312

[5] Gao Q H, Zhang Z Z, Zhao C, Wang Z X, Huo Y N, Xiang D, Jia C C, Guo X F 2024 *Adv. Photonics* **6** 064002

[6] Zhang Y, Wang L X 2011 *Acta Phys. Sin.* **60** 047304

[7] Whalley A C, Steigerwald M L, Guo X F, Nuckolls C 2007 *J. Am. Chem. Soc.* **129** 12590

[8] Jia C C, Migliore A, Xin N, Huang S Y, Wang J Y , Yang Q, Wang S P, Chen H L, Wang D M, Feng B Y, Liu Z R, Zhang G Y, Qu D H, Tian H, Ratner M A, Xu H Q, Nitzan A, Guo X F 2016 *Science* **352** 1443

[9] Xin N, Hu C, Sabea H A, Zhang M, Zhou C G, Meng L N, Jia C C, Gong Y, Li Y, Ke G J, He X Y, Selvanathan P, Norel L, Ratner M A, Liu Z R, Xiao S X, Rigaut S, Guo H, Guo X F 2021 *J. Am. Chem. Soc.* **143** 20811

[10] Gao M X, Wu R M, Zhang Y W, Meng Y S, Fang M M, Yang J, Li Z 2025 *J. Am. Chem. Soc.* **147** 2653

[11] Cao Y, Dong S H, Liu. S, Liu Z F, Guo X F 2013 *Angew. Chem. Int. Ed.* **52** 3906

[12] Tan M, Sun F, Zhao X Y, Zhao Z B, Zhang S R, Xu X N, Adijiang A, Zhang W, Wang H Y, Wang C K, Li Z L, Scheer E, Xiang D 2024 *J. Am. Chem. Soc.* **146** 6856

[13] Battacharyya S, Kibel A, Kodis G, Liddell P A, Gervaldo M, Gust D, Lindsay S 2011 *Nano Lett.* **11** 2709

[14] Zhou J F, Wang K, Xu B Q, Dubi Y 2018 *J. Am. Chem. Soc.* **140** 70

[15] Yoshida K, Shibata K, Hirakawa K 2015 *Phys. Rev. Lett.* **115** 138302

[16] Zhao Z K, Guo C Y, Ni L F, Zhao X Y, Zhang S R, Xiang D 2021 *Nanoscale Horiz.* **6** 386

[17] Liu H J, Chen L J, Zhang H, Yang Z Q, Ye J Y, Zhou P, Fang C, Xu W, Shi J, Liu J Y, Yang Y, Hong W J 2023 *Nat. Mater.* **22** 1007

[18] Lee S, Kim T, Kim H, Kim Y 2021 *ACS Appl. Polym. Mater.* **3** 6056

[19] Park C, Kim T, Kim H, Kim Y 2024 *J. Mater. Chem. C* **12** 16543

[20] Galperin M, Nitzan A 2005 *Phys. Rev. Lett.* **95** 206802

[21] Galperin M, Nitzan A 2006 *J. Chem. Phys.* **124** 234709

[22] FainbergB D, Jouravlev M, Nitzan A 2007 *Phys. Rev. B* **76** 245329

[23] FainbergB D, Sukharev M, Park T H, Galperin M 2011 *Phys. Rev. B* **83** 205425

[24] Cao H, Zhang M D, Tao T, Song M X, Zhang C Z 2015 *J. Chem. Phys.* **142** 084705

[25] Beltako K, Cavassilas N, Lannoo M, Michelini F 2019 *J. Phys. Chem. C* **123** 30885

[26] Selzer Y, Peskin U 2013 *J. Phys. Chem. C* **117** 22369

[27] Hao Y T, Lu Q X, Zhang Y L, Zhang M M, Liu X J, An Z 2024 *J. Chem. Phys.* **160** 184113

[28] Su W P, Schrieffer J R, Heeger A J 1979 *Phys. Rev. Lett.* **42** 1698

[29] Brazovskii S, Kirova N 2010 *Chem. Soc. Rev.* **39** 2453

[30] Zhang M M, Lu Q X, Liu X J, Gao K, An Z 2023 *Appl. Phys. Lett.* **123** 151102
[31] Zhang D C, Zuo L J, Ye L, Chen Z H, Wang Y, Xu R X, Zheng X, Yan Y J 2023 *J. Chem. Phys.* **158** 014106
[32] Li Z H, Tong N H, Zheng X, Hou D, Wei J H, Hu J, Yan Y J 2012 *Phys. Rev. Lett.* **109** 266403
[33] Jin J H, Zheng X, Yan Y J 2008 *J. Chem. Phys.* **128** 234703
[34] Kubis T, Vogl P 2011 *Phys. Rev. B* **83** 195304